Some numerical experiments with the finite element method to determine the shape factors for field permeability tests

François Duhaime
Department CGM – École Polytechnique, Montreal, Quebec, Canada
Robert P. Chapuis
Department CGM – École Polytechnique, Montreal, Quebec, Canada

ABSTRACT
Several authors have used the finite element method (FEM) to evaluate the shape factors used in the interpretation of in situ permeability test data. Apart from elements and grid sizes, authors rarely discuss the numerical aspect of shape factor calculations. This paper presents shape factor values obtained with the authors' FEM model programmed with MATLAB and two commercial FEM packages: SEEP and COMSOL. Proper grid and element sizes are discussed. The influence of the method used for flux integration, a usually hidden aspect of FEM calculations, is reviewed. Thiem's equation, an analytical solution to a problem similar to the one involved in shape factor calculations, is used to validate some of our conclusions. Our results indicate that Hvorslev's ellipsoid equation underestimates shape factor values by approximately 9 %.

RÉSUMÉ
Plusieurs auteurs ont utilisé la méthode des éléments finis (MEF) pour le calcul des coefficients de forme nécessaires à l'interprétation des résultats d'essais de perméabilité in situ. Mis à part la taille des éléments et les dimensions de la grille, ces auteurs présentent peu de détails quant à l'aspect numérique de leurs calculs. Cet article présente des valeurs de coefficients de forme obtenues avec un modèle d'éléments finis programmé par les auteurs avec MATLAB, et avec deux logiciels commerciaux : SEEP et COMSOL. Le choix de dimensions appropriées pour les éléments et le domaine de calcul est discuté. L'influence de la méthode utilisée pour intégrer le flux, un aspect peu étudié des éléments finis, est passée en revue. L'équation de Thiem, la solution analytique d'un problème similaire à celui du calcul des coefficients de forme, est utilisée pour valider certaines conclusions de l'article. Nos résultats indiquent que la formule de l'ellipsoïde de Hvorslev sous-estime les coefficients de forme d'environ 9 %.

1 INTRODUCTION

This paper deals with constant- and variable-head field permeability tests conducted in hydraulic piezometers or field permeameters. Various test configurations can be used. Figure 1 shows one example. For a constant-head test, we apply a constant hydraulic head and measure the flow rate in or out of the soil. For the variable-head test, water is either added or removed from the riser pipe and the water level movement toward its original position is recorded. The flow rate can then be computed with the water level change and the riser pipe section.

For permeability tests conducted in relatively stiff soils (e.g. dense sands and gravels), we can usually assume that the granular soil skeleton is perfectly rigid (Chapuis 1998). Darcy's law and the principle of mass conservation imply that the hydraulic head (h) field around the intake zone is a solution to Laplace's equation (Equation 1).

$$\nabla^2 h = 0 \qquad [1]$$

Harmonic functions, the family of solutions which satisfy Laplace's equation, have several interesting properties. The superposition property of harmonic functions implies that the rate of flow in or out of the cavity is directly proportional to the soil hydraulic conductivity (K), the difference between the water level in the riser pipe and the initial hydraulic head in the soil (H) and the shape factor (c) (Equation 2).

$$Q = -cKH \qquad [2]$$

The shape factor is a function of the intake zone geometry, of its L/D ratio (intake zone length / diameter) and of the recharge and impermeable boundaries surrounding the intake. Several methods have been used to define c throughout the years. In this paper, we present shape factor values obtained with the finite element method (FEM) for two common intake zone geometries. Our results cover a $2 \leq L/D \leq 20$ aspect ratio range.

The finite element method has been used in the past to obtain shape factor values. The main contribution of this paper is to dig deeper into the numerical aspects of shape factor calculations. Previous publications dealt with the influence of element and grid sizes on shape factor values (Chapuis 1989; Ratnam et al. 2001; Tavenas et al. 1990). In this paper, we show that the method used to integrate the flux in or out of the intake zone can also have its bearing on shape factor values. Results from a custom finite element program (MATLAB) are compared with those of two commercial finite element packages: COMSOL (COMSOL AB 2007) and SEEP (Geo-Slope International Ltd. 2008). Our shape factor values are generally in agreement with those that have been suggested in previous publications. We show that using

Hvorslev's (1951) ellipsoid formula for intake zones with L/D>2 results in a slight (generally < 13 %) underestimation of shape factor values and that this discrepancy can be corrected by changing Hvorslev's ellipsoid dimensions.

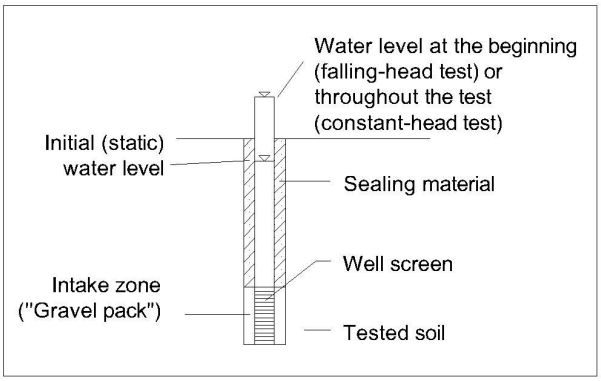

Figure 1. Permeability test in a hydraulic piezometer.

2 SHAPE FACTORS

Equation 2 implies that the shape factor is equal to the integral of the flux out of the intake zone and into the soil for a hydraulic conductivity of 1 m/s and a hydraulic head difference of 1 m.

For cylindrical intake zones, two axisymmetric geometries are of interest. Figure 2 shows the one which we will refer to as the impermeable bottom geometry. Water can only flow through the lateral surface of the cylinder. An impermeable borehole casing extends from both extremities of the intake zone. The self-boring permeameter of Tavenas et al. (1990) is an example of an apparatus where shape factor calculations would be based on this intake zone geometry. Figure 3 shows the permeable bottom geometry. Water can flow through both the lateral and bottom faces of the cylinder. An impermeable borehole casing extends upward. This geometry would be used to calculate shape factors for hydraulic piezometers like the one shown in Figure 1.

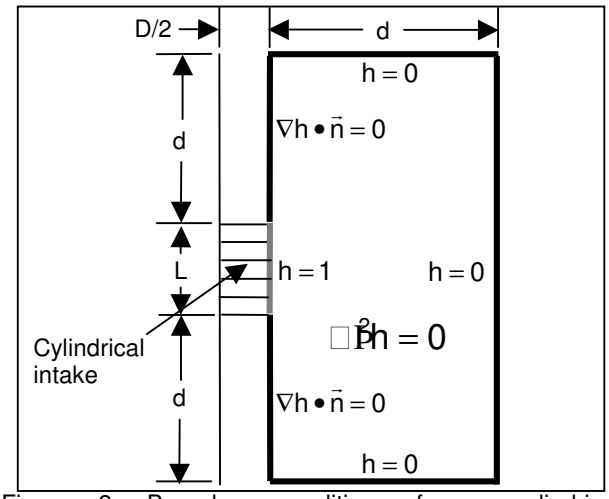

Figure 2. Boundary conditions for a cylindrical permeameter with an impermeable bottom.

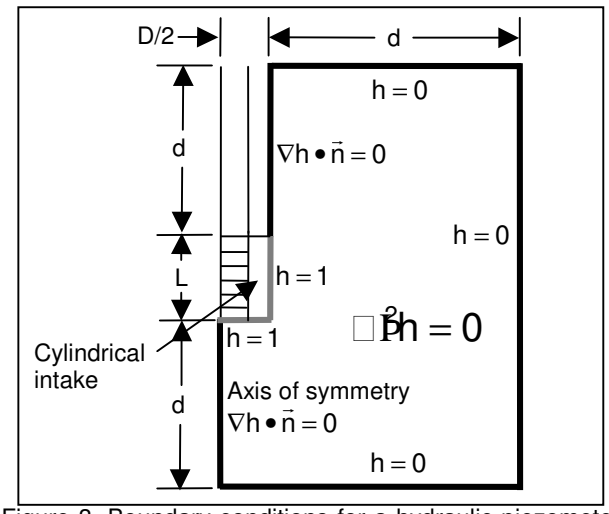

Figure 3. Boundary conditions for a hydraulic piezometer with a permeable bottom.

In both Figures 2 and 3, the domain in which the hydraulic head is a solution to Laplace's equation is bounded by a set of thicker lines. The thick grey lines outline the soil-intake zone interface while the thick black lines trace the impermeable boundaries ($\nabla h \bullet \vec{n} = 0$), axis of symmetry and distant constant head boundaries. If we use the usual assumption of an infinite soil medium, the domain dimension parameter d must tend toward infinity.

The boundary value problems of Figures 2 and 3 do not have analytical solutions. Four main approaches have been used to solve those problems and obtain shape factor values. The results obtained with the four methods for L/D > 2 are summarized in Figures 4 and 5.

The first method is to replace the cylindrical intake zone by an equivalent sphere or spheroid. An exact solution to the boundary value problem can then be found. Equation 3 is the so-called ellipsoid equation (Dachler 1936; Hvorslev 1951).

$$c = \frac{2\pi L}{\ln\left(\frac{L}{D} + \sqrt{1+\left(\frac{L}{D}\right)^2}\right)} \qquad [3]$$

To obtain this equation, the cylindrical intake zone is replaced by a prolate spheroid of focal length L and horizontal radius D/2. Equation 3 is usually assumed to be a good approximation of the boundary value problem of Figure 3 when L/D > 4 (Chapuis and Chenaf 2008). It is also often used when the geometry of Figure 2 applies, especially for large L/D ratio (Ratnam et al. 2001).

Other spheroid equivalents have also been presented. Maasland and Kirkham (1959) gave shape factors for a spheroid inscribed in the cylindrical intake zone. For L/D>2, the difference between their shape factor values and those given by Equation 3 is less than 5 %. Wilkinson (1968) suggested using a spheroid with approximately the same volume as the cylindrical intake zone. Shape factors for equal volume spheroids can be obtained by multiplying by 1.5 the L/D ratio in Equation 3. Randolph and Brooker (1982) obtained similar shape factor values

by using a spheroid with the same surface area as the cylindrical intake zone.

These equivalent geometries are seldom used in practice. Nonetheless, they can show the range of shape factor values resulting from a priori arbitrary equivalent spheroid dimensions. For L/D = 4, the shape factor values obtained with an equal volume spheroid and the inscribed spheroid differ by 28 %. Figures 4 and 5 show that the shape factor values obtained with the other methods lie between the values given by Wilkinson's (1968) and Hvorslev's (1951) spheroids.

The complete mathematical demonstration leading to Equation 3 is presented by Cassan (1980, p. 47). Similar developments lead to the other equivalent spheroids proposed in the literature. A closer examination of this proof shows that multiplying the spheroid radii by a constant multiplies the resulting shape factor by the same constant. This property will later be used to adjust the equivalent spheroid dimensions so that they match the shape factor values obtained from our finite element model.

The second of the four shape factor calculation methods applies to the boundary value problem of Figure 2. For this method, the constant head (Dirichlet) boundary condition along the soil-intake zone interface is replaced by an equivalent flux (Neumann) boundary condition. By using Fourier and Laplace transforms, a semi-analytical solution taking the general form of Equation 4 can be obtained (Dougherty and Babu 1984).

$$h(r,z) = \sum_{n=0}^{\infty} G_n K_0(a_n r)\cos(a_n z) \qquad [4]$$

$$a_n = \frac{1/2 + n}{L/2 + d}\pi \qquad [5]$$

Where K_0 is the zero order Bessel function of the second type. The G_n values depend on the chosen equivalent Neumann boundary. There are several ways to define this boundary condition. Randolph and Booker (1982) and Rehbinder (2005) used continuous functions while Mathias and Butler (2007) divided the boundary into segments each assigned with a constant flux value. The shape factors values derived using Mathias and Butler's (2007) discretization are shown in Figure 4.

3D electric analogs make up the third group of shape factor calculation methods. They are based on the analogy between the flow of water under Darcy's law and the flow of electricity according to Ohm's law (Schneebeli 1966, p.147). Shape factors are measured in a reservoir filled with water of a known electrical resistivity. Water replaces the soil medium. Constant hydraulic head surfaces and impermeable boundaries are replaced with electrical conductors and insulators. The intake zone is replaced by a cylindrical electrode. By applying a voltage between the intake zone electrode and the electrical conductor lining the reservoir, an electrical current is generated. Using the water resistivity, the measured electrical current and the applied voltage, an equivalent water flow rate can be calculated. Brand and Premchitt (1980) and Smiles and Youngs (1965) used this method

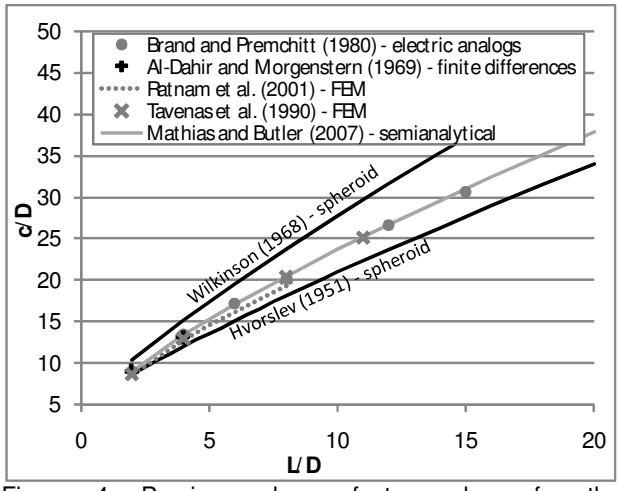

Figure 4. Previous shape factor values for the impermeable bottom geometry.

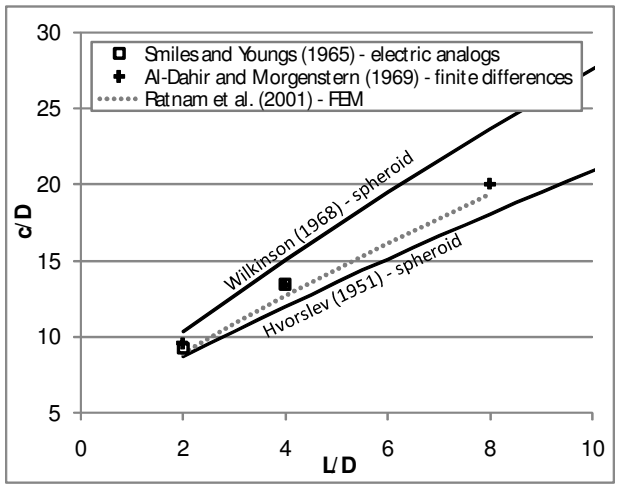

Figure 5. Previous shape factor values for the permeable bottom geometry.

to evaluate the shape factor of cylindrical intake zones. Their results are presented in Figures 4 and 5.

The fourth group of shape factor values are obtained with the finite difference (Al-Dhahir and Morgenstern 1969; Brand and Premchitt 1980) and finite element methods (Diène 1989; Ratnam et al. 2001; Tavenas et al. 1990). With both methods, approximate hydraulic head values are obtained for each node of a grid.

With the advent of relatively cheap and powerful personal computers, the use of numerical methods like the finite difference and finite element methods have become increasingly common. However, even when using a relatively robust commercial software package, users must remain prudent as numerical methods almost always generate an output, even if numerical errors are large or if the simulation input parameters are wrong. A direct consequence of this is that it can be difficult to judge if published numerical results are reliable when little information is presented on the methodology. Previous publications based on the finite difference and finite element methods mainly dealt with two numerical aspects of shape factor calculations: element and grid sizes.

For the impermeable bottom geometry, a linear trend between c and average element size at the soil-intake zone interface (t_{avg}) was observed. This trend was noticed for both the finite element and finite difference methods. Al-Dhahir and Morgenstern (1969), Brand and Premchitt (1980), Tavenas et al. (1990) and Ratnam et al. (2001) used this trend to estimate shape factor values for infinitely small t_{avg} values. Both Tavenas et al. (1990) and Al-Dhahir and Morgenstern (1969) used elements with a minimum t_{avg}/D ratio of approximately 0.1. They then used shape factor values obtained with coarser meshes to find a linear relation between c and t_{avg} and to extrapolate this relation to $t_{avg}=0$. For the permeable bottom geometry, Ratnam et al. (2001) noticed that the linear trend between c and t_{avg} was not always observed, especially for small L/D ratios. In these cases, they noticed that c was proportional to $t_{avg}^{1/4}$. They corrected their results based on this observation.

Chapuis (1989) warns us that the grid must be sufficiently large for the infinite medium hypothesis to be verified. If the grid is too small, gradients are overestimated since the hydraulic head must decrease more rapidly away from the intake zone to connect with closer boundary conditions. This also leads to overestimating the total flux and the shape factor. It must be noted that the choice of a grid size is also important for 3D electric analogs. The grid sizes used in previous publications can be compared using the d/D ratio (Figures 2 and 3). Tavenas et al. (1990) used a d/D ratio varying between 62.5 and 100. For their electric analogs measurements, Brand and Premchitt (1980) used a d/D ratio of approximately 150. Unfortunately, the grid size and the d/D ratio were not always stated explicitly in previous publications.

There are several ways to evaluate the influence of the chosen d/D ratio on shape factor values. Chapuis (1989) used image wells to obtain a corrected shape factor value (c') taking into account the finite grid size. The correction is based on the distance between the center of the intake zone and the recharge boundaries. For the boundary value problems of Figures 2 and 3, considering that d is much larger than L and D, the correction suggested by Chapuis (1989) can be rewritten as Equation 6.

$$c' = \frac{1}{1/c + 1/\pi d} \qquad [6]$$

Al-Dhahir and Morgenstern (1969) corrected their numerical shape factor values by calculating the shape factor for a spherical intake zone with the same surface area as the cylindrical intake zone. Since there is an analytical solution for the shape factor of a sphere in an infinite medium, the percentage error induced by a finite grid could be calculated and applied to the cylinder of equal surface area.

The main pitfall in using the FEM to calculate shape factor values is that this numerical method gives a good approximation of the field variable, in this case the hydraulic head, but not so much of its derivatives. When calculating c, it is those derivatives that we are evaluating. Unfortunately, little information on the methods used for flux integration was given in previous publications dealing with shape factor calculations.

Perhaps one of the only references to flux integration technique was made by Brand and Premchitt (1980). They mentioned using three different surfaces to integrate the flux around the intake zone. If we apply the divergence theorem to Equation 1, we notice that the volume of water entering or leaving a closed volume must cancel out. This is consistent with the principle of mass conservation from which Equation 1 originates. It implies that the flux can be integrated on an infinite number of surfaces surrounding the cylindrical intake zone. For example, if we apply the divergence theorem to the whole domain, the total fluxes at the soil-intake zone interface and at the distant boundaries must cancel out. Equation 7 then gives two different surfaces for which c can be calculated.

$$c = -\int_{\text{intake}} \nabla h \cdot \vec{n}\, d\Gamma = \int_{\text{distant boundary}} \nabla h \cdot \vec{n}\, d\Gamma \qquad [7]$$

Where $\vec{n}$ is a unit vector perpendicular to the boundary and pointing toward the outside and $d\Gamma$ is an infinitesimal surface element. As it will be shown in the next section, even on a given surface, there are more than one way to integrate the flux.

3 FINITE ELEMENT METHOD

Are presented in this section the equations for the finite element method and the two flux integration procedures that have been programmed for our MATLAB model.

3.1 Finite element equations

The mathematical development leading to the finite element equations can be found in any finite element textbook (e.g. Zienkiewicz et al. 2005). It is worthwhile to reproduce it here as it is the basis for the distinction between the two flux integration methods that have been programmed for the MATLAB model.

We start with Equation 1, multiply it by a test function w and integrate it over the domains bounded by thicker lines in Figures 2 and 3 (Ω). We get Equation 8.

$$\int_{\Omega} w \nabla^2 h\, d\Omega = 0 \qquad [8]$$

We then apply the divergence theorem to Equation 8 (Equation 9).

$$\int_{\Omega} \nabla w \cdot \nabla h\, d\Omega = \int_{\Gamma} w \nabla h \cdot \vec{n}\, d\Gamma \qquad [9]$$

h can then be replaced by its finite element approximation. For any element, this approximation can be written as Equation 10.

$$h \cong \sum_{j=1}^{6} \psi_j h_j \qquad [10]$$

Where Ψ_j is the interpolation function of node j and h_j is the FEM approximate value of h at node j. Locally, on each element, Ψ_j is the Lagrange polynomial equal to 1 at the j^{th} node and 0 at the other nodes. Globally, over Ω, Ψ_j is the piecewise combination of the local Lagrange polynomials of node j. Outside the elements which include node j, Ψ_j is equal to 0. Equation 10 is written assuming that quadratic triangular elements (6 nodes) are used. This is the type of elements we are using in our MATLAB model and for our simulations with SEEP and COMSOL.

For the Galerkin method, we also use the Ψ_j interpolation functions as test functions. By substituting Equation 10 and the test functions in Equation 9, we get Equation 11.

$$\sum_{j=1}^{NDDL} h_j \int_{\Omega} \nabla\psi_i \cdot \nabla\psi_j \, d\Omega = \int_{\Gamma} \psi_i \nabla h \cdot \vec{n} \, d\Gamma \qquad [11]$$

Where NDDL is the total number of nodes over Ω. Since we have one test function per node, Equation 11 can be rewritten as a system of NDDL equations, one for each test function (Equation 12).

$$\mathbf{AH} = \mathbf{S} \qquad [12]$$

Where **H** and **S** are vectors containing the h_j values and the right-hand side members of each equation. We will later refer to the **S** vector entries as the secondary variables. The entries of matrix **A** are calculated with Equation 13.

$$A_{ij} = \int_{\Omega} \nabla\psi_i \cdot \nabla\psi_j \, d\Omega \qquad [13]$$

For the nodes on Γ, we either know h_j (constant-head boundaries) or the secondary variable (no-flow boundaries). For nodes on no-flow boundaries, the secondary variables are equal to 0. The entries of S are also equal to 0 for the inside nodes. We therefore have as many unknowns as we have equations. The system of Equation 12 can be solved. Both the unknown secondary variables and unknown approximate head values can be calculated.

Implementation of the finite element method requires a few more steps, the most important being the coordinates transformation (Zienkiewicz et al. 2005, p.145). This step facilitates the numerical integration of Equation 12 for each element. Coordinates transformation will not be reproduced here as Equation 12 is sufficient to explain the difference between our two flux integration methods.

3.2 Flux integration

The first flux integration method will be referred to as the field variable method. It is based on the substitution of the finite element approximation (Equation 10) in the flux integral (Equation 7). For example, at the soil-intake zone interface, we get Equation 14.

$$c = -\int_{intake} \nabla h \cdot \vec{n} \, d\Gamma \cong -\sum_{j=1}^{NDDL} h_j \int_{intake} \nabla\psi_j \cdot \vec{n} \, d\Gamma \qquad [14]$$

The only interpolation functions which will contribute to this integral are those of the triangular elements with a side matching the part of Γ on the soil-intake zone interface.

The second method utilizes the secondary variables. If we assume that the flux is locally constant around each node of the soil-intake zone interface, the right-hand side of Equation 11 can be rewritten as follows (Equation 15).

$$S_i = \nabla h \cdot \vec{n} \int_{intake} \psi_i \, d\Gamma \qquad [15]$$

For each node on the interface, the assumed constant flux value can be calculated by dividing the secondary variable by the integral of the corresponding interpolation function.

$$\nabla h \cdot \vec{n} = \frac{S_i}{\int_{\Gamma} \psi_i \, d\Gamma} \qquad [16]$$

To integrate the flux, we must assign a tributary surface area to each node on the interface. The constant flux value of each node can then be applied to these surface areas.

Based on the two shape factor definitions proposed in Equation 7, we have chosen to integrate the flux both on the soil-intake zone interface and at the distant boundaries. Applying the two methods at both boundaries gives 4 shape factor values per numerical simulation.

3.3 Mesh

Previous shape factor calculations with the finite element and finite difference methods were conducted using smaller node spacings in the neighbourhood of the soil-intake zone interface, especially around the transition from constant-head to impermeable boundary conditions (Al-Dhahir and Morgenstern 1969; Ratnam et al. 2001; Tavenas et al. 1990). However, exact element size distributions as a function of radial distance and elevation and the rationale behind these size distribution choices were not always presented.

The element size distribution used for our MATLAB model is based on a distribution generated with COMSOL's adaptive meshing solver (Figure 6). With adaptive meshing, element sizes are chosen so that the contribution of each element to the finite element approximation error is approximately equal (Zienkiewicz et al. 2005). Figure 6 shows that for the permeable bottom geometry, finer elements are generated around the intersection of the intake zone bottom and cylindrical surface (Point P_1). Finer elements are also generated at the top of the soil-intake zone interface, where the boundary conditions change from constant-head to impermeable (Point P_2). Similar element size distributions are obtained for the impermeable bottom geometry.

Globally, the relationship between element size and distance from the intake zone is roughly linear.

We have used the meshing algorithm of Persson and Strang (2004) to generate meshes for our MATLAB model. This algorithm allows the average element size to be defined as a function of radial and vertical coordinates. For both the permeable and impermeable bottom geometries, the element size distribution for intake zones with aspect ratios L/D≥4 is given by Equation 17.

$$t \approx t_0 + 0.025r \qquad [17]$$

Where t_0 is the size (in meters) of the smallest elements around the intake zone and r is the minimum distance (in meters) between the point where element size is estimated and points P_1 and P_2 of Figure 6. Our final results were obtained with t_0 = 0.00225 m. This minimum element size produced meshes with between 71 000 and 88 000 elements.

Smaller elements were used for intake zones with aspect ratios L/D<4 (Equation 18).

$$t \approx t_0 + 0.018r \qquad [18]$$

A minimum t_0 value of 0.0016 m was used. Between 123 000 and 128 000 elements were generated.

We calculated shape factor values for increasing d values (Figures 2 and 3) to choose a sufficiently large grid for the infinite medium hypothesis to be verified. Since larger intake zones are more sensitive to grid size, L/D=20 was used (Figure 7). For L/D≥4, d=40 m was chosen for the final simulations. For intake zones with smaller aspect ratios, d=30 m was used. Equation 6 was used to correct the final shape factor values. Even if d is large with respect to the chosen intake zone diameter (D=11 cm, d/D≈360), the correction amounts to 3.3 % of the shape factor value for L/D=20.

Figure 8 shows one of the meshes used to obtain our final results with the MATLAB model.

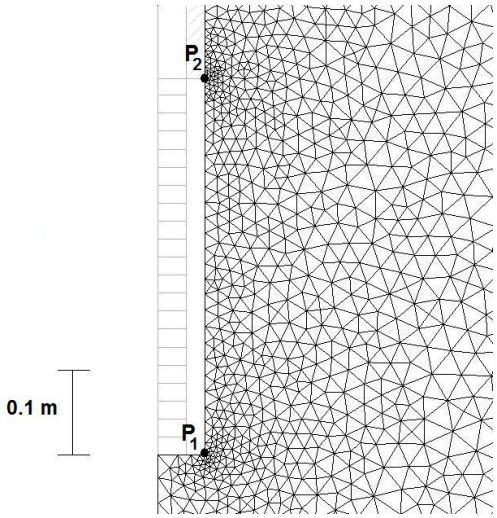

Figure 6. Detailed view of the meshing around the intake zone (COMSOL's adaptive meshing solver, L/D = 4). This mesh has approximately 1.7 times less elements than the meshes used to obtain the results of Figures 12 and 13.

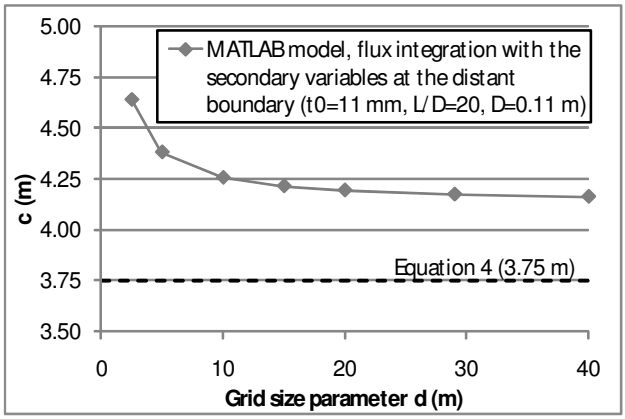

Figure 7. The influence of grid size on shape factor values (impermeable bottom geometry).

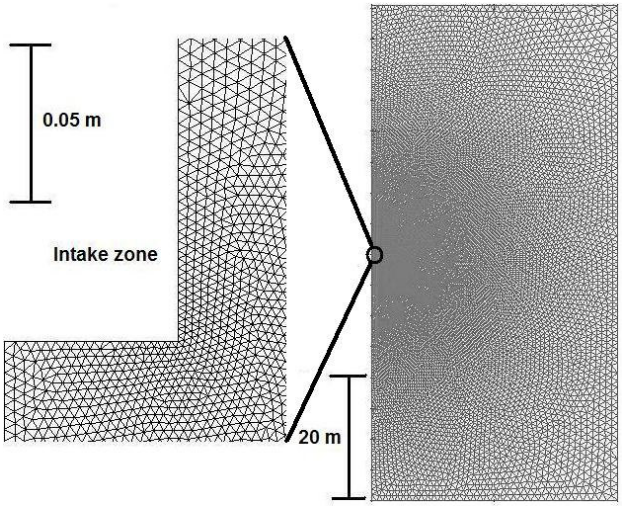

Figure 8. MATLAB mesh example (permeable bottom, L/D=4, D=0.110 m, d=40 m and t_0=0.00225 m).

4 RESULTS AND DISCUSSION

Thiem's (1906) equation was used to test our two flux integration techniques. Assuming steady state conditions and the applicability of Darcy's law, Equation 19 is the exact solution to the problem of radial flow toward a well fully penetrating a confined aquifer circumscribed by a cylindrical constant-head boundary.

$$Q = \frac{2\pi b}{\ln(2R/D)} KH \qquad [19]$$

The cylindrical constant-head boundary is located at a radial distance R from the center of a well of diameter D, b is the confined aquifer thickness and H is the head difference between the well and the constant-head boundary. Equation 19 can also be expressed as the product of a shape factor, K and H.

Figure 9 compares Thiem's solution with shape factor values obtained with the field variable and secondary variable techniques for different element sizes (t_{avg}). For the secondary variable technique, the FEM solution converges very rapidly to the analytical solution. With a

t_{avg}/D ratio of 1, it is within 0.5 % of the exact solution. On the other hand, convergence with field variable derivatives is much slower. Simulations conducted with COMSOL and SEEP also show variable rates of convergence (Figure 9).

Figure 10 shows that the same conclusions apply to the shape factor of the impermeable bottom geometry. In this case, we used the same intake zone geometry and grid size as Tavenas et al. (1990) to compare the rates of convergence. Figure 10 shows that the flux integration technique of Tavenas et al. (1990) converges at the same rate as our field variable derivatives method.

Figure 11 shows that at the distant boundaries, the field variable derivatives and secondary variable method converge rapidly to the same result. This was the case for all our simulations.

For the permeable bottom geometry, the convergence of the secondary variable method was not as rapid (Figure 11). This could be linked to the different convergence rate observed for this geometry and for a low L/D ratio by Ratnam et al. (2001).

In light of our tests with flux integration methods, we notice that different methods will give different results and that there is sometimes an optimal way to integrate the flux. To get our definitive shape factor values, we have used the secondary variable technique with integration at the distant boundary. With COMSOL, integration is performed at the distant boundaries. With SEEP, flux sections a few meters from the intake are used.

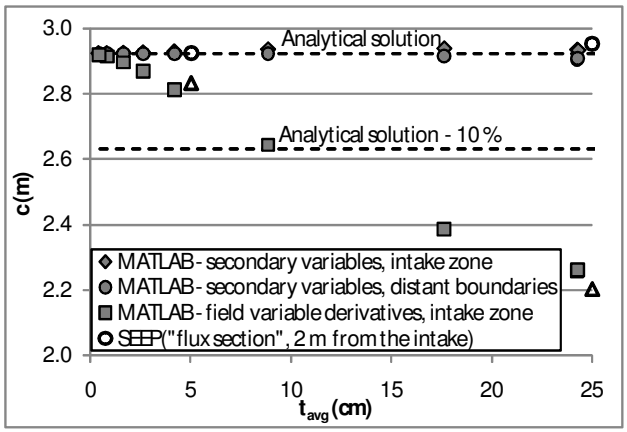

Figure 9. Shape factor for Thiem's equation (D=0.110, b=2 m, R=4 m).

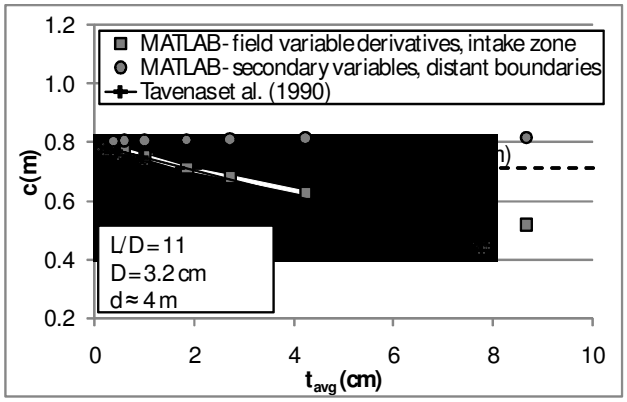

Figure 10. Shape factor as a function of mean element size around the intake zone, impermeable bottom geometry.

Figures 12 and 13 present the shape factor values obtained with our MATLAB model, COMSOL and SEEP. For the calculations with SEEP and COMSOL, grids of 40 m were used. With SEEP, a different intake diameter (5 cm) was used to make sure that our results were diameter independent. Elements of approximately 1 mm were used on the soil-intake zone interface. With COMSOL, elements of around 6 mm were generated at the interface. Results obtained with COMSOL and SEEP were also corrected with Equation 6.

As in previous investigations (Figures 4 and 5), our results plot between the spheroids of Wilkinson (1968) and Hvorslev (1951). The maximum deviations with respect to the spheroid of Hvorslev (1951) are respectively 12.6% and 8.9% for the permeable and impermeable bottom geometries. In both cases, these maximum errors occur for intermediate L/D ratios (4-10).

The spheroids which give the best fits on our FEM results are obtained by multiplying Equation 3 and the spheroid's radii by 1.098 and 1.082 for the permeable and impermeable bottom geometries (Figures 12 and 13). For $2 \leq L/D \leq 20$, if we use an average factor of 1.09 for both geometries, the maximum error is 6.2% for the impermeable bottom geometry. This maximum error is observed for low L/D ratios: for L/D>4, the error is under 2.5%.

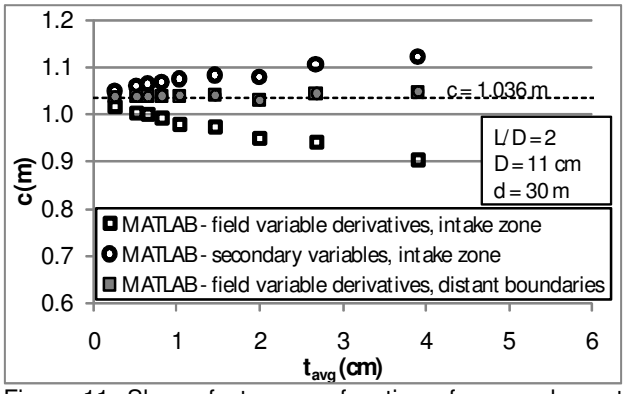

Figure 11. Shape factor as a function of mean element size around the intake zone, permeable bottom geometry.

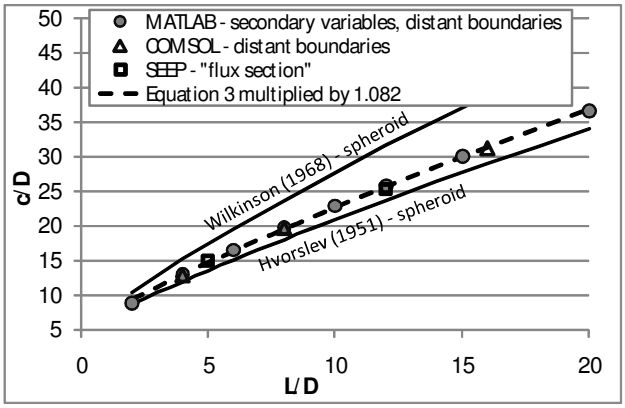

Figure 12. Shape factor values for impermeable bottom geometry.

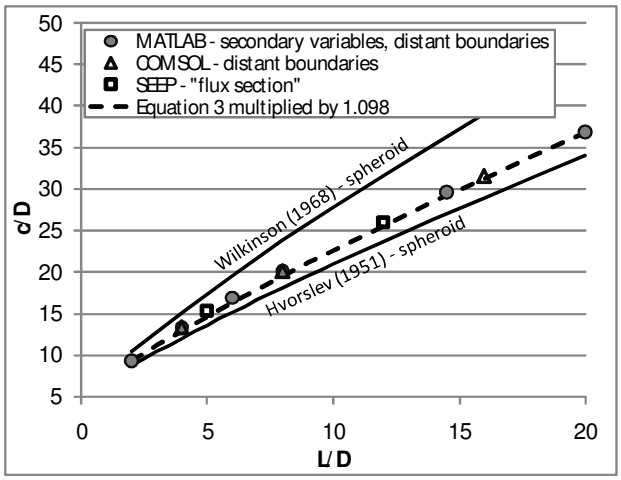

Figure 13. Shape factor values for the permeable bottom geometry

5 CONCLUSION

There are several methods to integrate fluxes with the finite element method. Our numerical tests show that these methods give different results and convergence rates.

Our numerical values show that Equation 3, in its original form or after the dilation suggested in this paper, gives reliable shape factor values. For $2 \leq L/D \leq 20$ and for both the permeable and impermeable bottom geometries, multiplying Equation 3 by 1.09 limits the error on shape factor values to approximately 6.2 %. If the uncorrected version of Equation 3 is used, the deviation reaches 12.6 %. These errors are deemed insignificant considering that field permeability tests are error prone and considering that the errors due to the infinite and infinitely rigid medium hypothesis are probably more important than 12.6 %.

ACKNOWLEDGEMENTS

Research for this paper was sponsored by the Natural Sciences and Engineering Research Council of Canada.

REFERENCES

Al-Dhahir, Z.A., and Morgenstern, N.R. 1969. Intake factors for cylindrical piezometers tips. *Soil Science*, 107: 17-21.

Brand, E.W., and Premchitt, J. 1980. Shape factors of cylindrical piezometers. *Geotechnique*, 30(4): 369-384.

Cassan, M. 1980. *Les essais d'eau dans la reconnaissance des sols*. Eyrolles, Paris, France.

Chapuis, R.P. 1989. Shape factors for permeability tests in boreholes and piezometers. *Ground Water*, 27(5): 647-654.

Chapuis, R.P. 1998. Overdamped slug test in monitoring wells: review of interpretation methods with mathematical, physical, and numerical analysis of storativity influence. *Canadian Geotechnical Journal*, 35: 697-719.

Chapuis, R.P., and Chenaf, D. 2008. Comment on "Shape factors for constant-head double-packer permeameters" by S. A. Mathias and A. P. Butler. *Water Resources Research*, 44(7): W07601.

COMSOL AB 2007. *COMSOL Multiphysics user's guide*. COMSOL AB, Stockholm, Sweden.

Dachler, R. 1936. *Grundwasserstromung (Flow of groundwater)*. Julius Springer, Vienna, Austria.

Diène, M. 1989. Mesure in situ de la perméabilité des argiles. Ph.D., Université Laval, Quebec city, QC, Canada.

Dougherty, D.E., and Babu, D.K. 1984. Flow to a partially penetrating well in a double-porosity reservoir. *Water Resources Research*, 20(8): 1116-1122.

Geo-Slope International Ltd. 2008. *Seepage Modeling with SEEP/W 2007*. Geo-Slope International Ltd., Calgary, AB, Canada.

Hvorslev, M.J. 1951. *Time-lag and soil permeability in ground water observations, Bulletin 36*. U.S. Army Engineering Waterways Experimental Station, Vicksburg, MS, USA.

Maasland, M., and Kirkham, D. 1959. Measurement of permeability of tri-axially anisotropic soil. *ASCE, Journal of the Soil Mechanics and Foundations Division*, 85(SM 3): 25-34.

Mathias, S.A., and Butler, A.P. 2007. Shape factors for constant-head double-packer permeameters. *Water Resources Research*, 43(6): W06430.

Persson, P.-O., and Strang, G. 2004. A simple mesh generator in MATLAB. *SIAM Review*, 46(2): 329-345.

Randolph, M.F., and Brooker, J.R. 1982. Analysis of seepage into a cylindrical permeameter. *In Proceedings of the 4th International Conference on Numerical Methods in Geomechanics*. Edmonton, AB, Canada, Vol.1: 349-357.

Ratnam, S., Soga, K., and Whittle, R.W. 2001. Revisiting Hvorslev's intake factors using the finite element method. *Geotechnique*, 51(7): 641-645.

Rehbinder, G. 2005. Relation between non-steady supply pressure and flux for a double packer conductivity meter: an approximate analytical solution. *Flow, Turbulence and Combustion*, 74(1): 1-20.

Schneebeli, G. 1966. *Hydraulique souterraine*. Eyrolles, Paris, France.

Smiles, D.E., and Youngs, E.G. 1965. Hydraulic conductivity determinations by several field methods in a sand tank. *Soil Science*, 99(2): 83-87.

Tavenas, F., Diene, M., and Leroueil, S. 1990. Analysis of the in situ constant-head permeability test in clays. *Canadian Geotechnical Journal*, 27(3): 305-314.

Thiem, G. 1906. *Hydrologische Methoden*. Gebhardt, Leipzig, Germany.

Wilkinson, W.B. 1968. Constant head in situ permeability tests in clay strata. *Geotechnique*, 18(2): 172-194.

Zienkiewicz, O.C., Taylor, R.L., and Zhu, J.Z. 2005. *The finite element method : its basis and fundamentals*. Elsevier Butterworth-Heinemann, Boston, MA, USA.